RSC Advances

ROYAL SOCIETY OF CHEMISTRY

www.rsc.org/advances

Graphical abstract

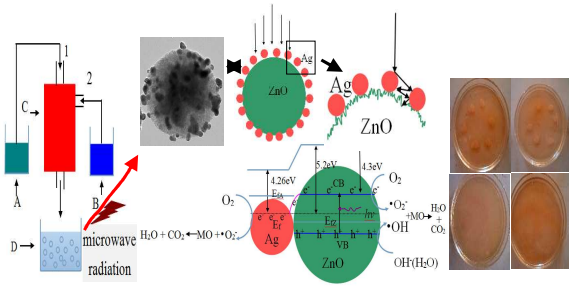

A continuous concentric impinging stream method was used for preparing ZnO/Ag MNSs , which possessed excellent photocatalytic and antibacterial activities.

ZnO/Ag micro/nanospheres with Enhanced Photocatalytic and Antibacterial Properties Synthesized by a Novel Continuous Synthesis Method

Zhenjiang Li[a, b], Fenghua Zhang[a], Alan Meng[c, *], Cuicui Xie[b], Jing Xing[c]

[a] *Key Laboratory of Nanostructured Materials, College of Materials Science and Engineering, Qingdao University of Science and Technology, Qingdao 266042, Shandong, P. R. China.*
[b] *Key Laboratory of Polymer Material Advanced Manufacturings Technology of Shandong Provincial, Qingdao University of Science and Technology, Qingdao 266061, Shandong, P. R. China.*
[c] *State Key Laboratory Base of Eco-chemical Engineering, College of Chemistry and Molecular Engineering, Qingdao University of Science and Technology, Qingdao 266042, Shandong, P. R. China.*
[*] *Corresponding author: Corresponding author at: 53 Zhengzhou Road Qingdao 266042, Shandong, PR China.*
Tel.: +86 532 88956228; fax: +86 532 88956228.
E-mail address: alanmengqust@163.com.

Abstract

A series of ZnO/Ag micro/nanospheres (MNSs) with different Ag contents have been successfully synthesized via a self-design concentric impinging stream microreactor combined with microwave technique. Various characterization results showed that Ag nanoparticles with the average diameter of about 15 nm were successfully deposited upon ZnO microspheres with sizes ranging from 300-700nm which are composed of ZnO nanoparticles with diameter of less than 10 nm. The photocatalytic performance of a series of ZnO/Ag MNSs was evaluated against methyl orange, and the antibacterial property was tested against Escherichia coli. All

of the results showed that the photocatalytic and antibacterial activities of ZnO/Ag MNSs loaded with different Ag contents are superior to that of the pure ZnO. The optimal loading Ag content is approximately 7.5 atom % as the MO is almost completely degraded irradiated for 30 min and the MIC value is 100 $\mu g \cdot mL^{-1}$. The possible mechanisms of the enhanced photocatalytic and antibacterial property of ZnO/Ag MNSs were proposed. This fabrication method has the inherent advantages of simplicity, continuous production and low cost, so it is more appropriate for a large-scale continuous production with higher yields of ZnO/Ag MNSs in industry.

1.Introduction

In recent years, the prevention of toxic chemical and microbial contamination is essential in the health care system. Therefore, the development of effective material having both photocatalytic and antimicrobial properties is of great significance. Many studies show that zinc oxide (ZnO) can be widely applied in environmental remediation because of their availability, nontoxicity, stability, low cost and environmental friendliness[1-3]. ZnO has been widely studied in photocatalysts, photoconductor, piezoelectric and gas sensing devices, and in medical use, due to its unique properties and aesthetic morphologies[4-8]. Further, it is a bactericide and is effective to inhibit both Gram-positive and Gram-negative bacteria[9-11].

However, the high recombination ratio of photoinduced electro-hole pairs has hindered the application of ZnO. The deposition of noble metals, such as Ag, Au, Pt, Cu, Ce, and Ga, onto ZnO can effectively improve the photocatalytic activity of ZnO[12-17]. It is achieved due to the electron transfer from ZnO to the metal nanoparticles, which decreases the number of electron-hole recombination events, thus enhancing the photocatalytic activity.

Among the noble metal/ZnO nanoparticles, Ag/ZnO has attracted particular attention for their low cost and the superior properties. The present works reveal larger photocatalytic and bactericidal activities of Ag-doped ZnO.[18-21] Not only because the hybridization of ZnO with Ag increases the rate of electron-transfer under UV irradiation, resulting in a better photocatalytic activity compared with that of pure ZnO NPs, but also because Ag is effective in deactivating and inhibiting growth of

both Gram negative and Gram positive bacteria. Because of this, combining Ag with ZnO, would produce a material with strong antibacterial properties for both Gram negative and Gram positive bacteria, and hence will expand the antibacterial activities of materials to a wider variety of applications. There are several methods on the synthesis of ZnO/Ag nanoparticles such as wet chemical method, [22] solvothermal method,[23] photoreduction method,[24] hydrothermal method,[25] microwave,[26] nonionic polymer assisted thermolysis[27]. However, the disadvantage in using the nanoparticles is due to their potential dangers associated with their size which can affect humans and the environment. Considering that disadvantage of nanoparticles, Ag nanoparticles loaded onto ZnO microspheres can avoid these disadvantages. During the past several years, some of methods have been developed for the preparation of ZnO/Ag MNSs, such as hydrothermal,[28] solvothermal,[29] magnetron sputtering,[30] thermal decomposition,[31] and so on. However, these methods are often based on tedious operations and rigorous experimental conditions, so it can be unable to large-scale continuous production and not suitable for industrialization. Moreover, these methods often lack good control of particle size and morphology, and which have the low yield and the high energy consumption.

Thus, developing a facile method to construct metal-oxide micro-nanocomposites with outstanding performance is needed. Chemical reactions performed in microreactors would meet the requirement, and can control the size and structure. However, some common microreactors have many disadvantages such as low surface to volume ratio, low-yield, inefficient heat transfer and less molecular-diffusion[32-36].

So it is limited for practical application.

In this research, a series of ZnO/Ag MNSs with different Ag contents have been synthesized by using self-design a concentric impinging stream microreactor combined with microwave technique. Compared with the literature report, the concentric impinging stream microreactor consist of a series of channels (700 μm in diameter), which possesses a high surface and reaction volumes. A series of channels provide reaction volumes that are more homogeneous with respect to concentration, temperature, and mass transport, leading to a highly efficient and better control of the reaction, and more uniform particles are generated. Additionally, the method shows reduced reaction time, yield improvement, large-scale continuous production, and more suitable for the industrialization. In the paper, both the photocatalytic activity and the antibacterial activity of a series of ZnO/Ag MNSs were evaluated. The results showed that the ZnO/Ag MNSs, especially with 7.5 atom% of Ag, possessed excellent photocatalytic activity and antibacterial activity. The possible mechanism of the enhanced photocatalytic and antibacterial activity of ZnO/Ag MNSs are also presented. This work not only provides a highly efficient and large-scale continuous production methods of ZnO/Ag MNSs, also can provide beneficial reference for other composite materials in terms of synthesis technology.

2.Experiment Section

2.1. Materials

Zinc nitrate hexahydrate ($Zn(NO_3)_2$•$6H_2O$), silver nitrate ($AgNO_3$), sodium hydroxide (NaOH)，sodium citrate（$C_6H_5Na_3O_7 \cdot 2H_2O$）and alcohol were used as the

raw material. Methyl orange (MO) was used as the model dye for photocatalytic studies. The phosphate buffer solution (PBS) was made up of 8.0 g NaCl, 0.2 g KCl, 3.63 g $Na_2HPO_4•12H_2O$ and 0.24 g KH_2PO_4 in 1 L deionized water and adjusted to a desired pH. They were all purchased from the Sinopharm Chemical Reagent Co. Ltd. Nutrient Broth and Nutrient Agar was purchased from Qingdao Hope Biol-Technology Co. Ltd, China. All the chemicals were of analytical grade and used without any further purification. Deionized water was used in all experiment.

2.2. Preparation of ZnO/Ag micro/nanospheres

Firstly, 0.1 mol of NaOH and 0.05 mol of $C_6H_5O_7Na_3$ were dissolved in 250 mL of deionized water to form a mixed solution (A). 0.05 mol of $Zn(NO_3)_2$ and a suitable amount of $AgNO_3$ were dissolved in 250 mL of deionized water to form a mixed solution (B). In order to investigate the effect of Ag contents on the properties of Ag/ZnO MNSs, the Ag content was adjusted as 0, 2.5, 5.0, 7.5, and 10.0 atom%. The as-obtained solutions A and B were respectively put into the containers in Figure 1, which were preheated to 80°C. Then, they were pumped into the 1 and 2 inlets of Figure 1 and reacted in the self-design concentric impinging streams microreactor. The formed precipitate was collected and was performed under microwave irradiation (300 W) with magnetic stirring at 1200 r/min at 80 ℃ for 60 min. Then, the precipitations were washed several times with deionized water and ethanol, respectively, and oven-dried at 60°C for 6 h. Finally, the ZnO/Ag micro/nanospheres were obtained. The Figure 2 shows the whole flowchart schematic.

2.3. Characterization

X-ray diffractometer (XRD, D/MAX-2500/PC X-ray diffractometer, Rigaku, Akishima-Shi, Japan) was used to analyze the crystalline structure of the ZnO microspheres with various Ag contents. The morphology and composition of the products was characterized by transmission electron microscopy (TEM, JEM-2000EX, Japan) and scanning electron microscopy (SEM, JEOL JSM-6460LV, Tokyo, Japan) equipped with energy dispersive spectrometer (EDS). The UV–visible spectra of a series of ZnO/Ag micro/nanospheres with different Ag contents were obtained using a UV-visible spectrometer (Lambda 35, PerkinElmer, USA) over the range of 200-700nm, while photoluminescence at room temperature was recorded on a Hitachi F-4500 FL spectrophotometer.

2.4. Photocatalytic activity measurements

The photocatalytic activity was evaluated by measuring the decomposition of the methyl orange (MO) solution with a concentration of 10 mg/L. 10 mg of ZnO/Ag micro/nanospheres photocatalyst was added to 10 mL MO aqueous solution and dispersed under ultrasonic vibration for 5 min and then magnetic stirring for 30 min in darkness to ensure the establishment of an adsorption-desorption equilibrium between the photocatalyst and the MO aqueous solution. The degradation of MO aqueous was carried out in a XPA-VII type photochemical reaction device (Xujiang electromechanical factory, Nanjing). A 100 W mercury lamp was employed as UV light source (λ<400 nm). Aliquots were taken from the suspension at regular time intervals. The photodegradation efficiency was monitored with a UV-vis spectrometer (Lambda 35, PerkinElmer) by measuring the absorbance of the solution at the

maximum absorption wavelength (457 nm) at room temperature.

2.5. Antibacterial property test

The antimicrobial activities of the samples were tested through the determination of the minimum inhibitory concentration (MIC) as a qualitative measure of cell growth. Escherichia coli were used to test the antimicrobial activities of ZnO/Ag MNSs. To examine the bacterial growth rate, the Escherichia coli bacteria were grown in Nutrient Agar medium supplemented with various concentrations of ZnO/Ag colloidal suspensions. The ZnO/Ag MNSs with different Ag contents was dispersed in PBS (10 mg/ml). Further dilutions were prepared at the required quantities of 50, 100, 150, 200, 300, 400 and 500μg/ml concentrations. Nutrient Agar, which contained tested samples and controls, were inoculated with approximately 5×10^5 cfu/ml of actively dividing bacterial, and incubated at 37 °C for 24 h. The controls containing the bacteria without the test materials were also included. The MIC was defined as the lowest concentration required to arrest the growth of the bacteria at the end of 24 h of incubation. All antibacterial tests were carried out in triplicate and the averages are reported.

3.Results and discussion

3.1. Crystal structure and morphology

The X-ray diffraction (XRD) patterns of a series of samples with different Ag contents are shown in Figure 3. All of the diffraction peaks are consistent with the standard data of typical wurtzite structure of ZnO (JCPDS Card File No. 36-1451) and face centered cubic (fcc) silver (JCPDS Card File No. 04-0783). With the addition of

Ag content, the diffraction peaks of Ag increase, implying more Ag particles deposited onto the surface of ZnO. No other crystalline impurities are observed. In addition, there is no remarkable shift of all diffraction peaks which indicated that silver atoms are not incorporated into the ZnO lattice.

In order to obtain detailed information about the microstructure and morphology, SEM, TEM and HRTEM of ZnO/Ag MNSs with 7.5 atom % Ag were carried out and shown in Figure 4. Scanning electron microscopy (SEM) (Figure 4(a)) shows near spherically shaped particles in 300-700nm diameter. The energy dispersive spectrum (EDS) (inset of Figure 4(a)) confirms the presence of Ag, O and Zn with an atomic ratio of ~3:40, which is consistent with the above XRD results. The EDS analysis revealed that the Ag content of the synthesized samples is close to the theoretical values. Transmission electron microscopy (TEM) was used to observe the distribution of the Ag particles, shown in Figure 4(b). Various Ag nanoparticles with the average diameter of about 15 nm were deposited on the surface of ZnO microsphere. The Figure 4(c) is the HRTEM image of the interface between the ZnO and Ag. We can find that the surface of the ZnO is rough, consisted of the numerous of ZnO nano grains with diameter of less than 10 nm, which increased the area of the catalytic reaction. Figure 4(d) shows a HRTEM image from the squared region of Figure 4(c), and the crystal lattice can be observed directly. The plane fringe with a 0.2359 nm crystalline plane spacing is assigned to the Ag (111) planes. The plane fringe with 0.2814 nm and 0.2476 nm crystalline plane spacing is assigned to the ZnO (100) and (101) planes, which indicates that the ZnO nano grains are growing along different

directions. Two insets of Figure 4(d) are the SAED patterns of the “e” and “f” area of Figure 4(c), respectively. Inset Figure 4(e) and Figure 4(f) shows that Ag nanoparticle is a single crystal and the ZnO is polycrystal consisted of the numerous of single hexagonal wurtzite crystals.

On the basis of the above observations, a possible growth mechanism of the ZnO/Ag micro/nanospheres is proposed in Figure 5. In the early stage of the reaction (Figure 5(a)), the ZnO nanoparticles formed quickly. However the obtained ZnO nanoparticles was not stable in the mixed aqueous solution and grew larger and self-assembled to ZnO microspheres (Figure 5(b)) easily and quickly to reduce the surface energy with the assistance of sodium citrate. At the same time, the reaction between OH^- and Ag^+ may occur, leading to the formation of Ag_2O nuclei deposited on the surface of ZnO microspheres (Figure 5(c)). In this reaction procedure (Figure 5(d)), the added sodium citrate acted not only as stabilizer but also as reducing agent to reduce Ag^+ into Ag. On the one hand, Ag_2O on the surface of ZnO microspheres can be reduced by sodium citrate to form the tiny Ag particles for subsequent growth of Ag particles under microwave irradiation, on the other hand, As the reaction continued, the sodium citrate would reduce more Ag+ and thus more Ag nuclei are formed on the surface of ZnO microspheres, and Ag nanoparticles will be grew on Ag nuclei. Ag nanoparticles were gradually deposited on the surface of ZnO microspheres leading to the formation of ZnO/Ag micro/nanospheres(Figure 5(e)).

The XPS analysis was carried out to investigate the surface structure of the ZnO/Ag MNSs and the results are shown in Figure 6. The binding energies in the XPS spectra are calibrated by using that of C 1s (284.8 eV). All peaks in the XPS full spectrum shown in Figure 6 (a) can be ascribed to Zn, Ag, O, and C elements and no peaks of

other elements were observed. The presence of C comes mainly from pump oil in the vacuum system of the XPS equipment. It is indicated that the ZnO/Ag MNSs is only composed of three elements Zn, O and Ag, which is consistent with the above XRD and EDS results. The high resolution spectra for Zn, O, and Ag species are shown in Figures 6 (b), (c), and (d), respectively. In Figures 6 (b) and (c), the peaks profiles are symmetric and center at 1021.2 and 530.1 eV, which are attributed to Zn 2p 3/2 and O 1s of ZnO specimen, respectively. [37, 38] The Ag 3d 5/2 peak appears at a binding energy of 367.2 eV, and the splitting of the 3d doublet is 6.05 eV, indicating the metallic nature of silver. [39] Interestingly, the binding energies of Ag 3d 5/2 and Ag 3d 3/2 are367.2 eV and 373.25 eV for the ZnO/Ag MNSs, which shift to the lower binding energy compared with the corresponding values of bulk Ag (the standard binding energies of Ag 3d 5/2 and Ag 3d 3/2 for bulk Ag are about 368.2 and 374.2 eV, [37] respectively). This confirms the interaction between Ag and ZnO nanocrystals as the binding energy of monovalent Ag is known to be much lower than that of zerovalent Ag. Similar results were also found in Zheng's work. [40]

3.2. Photocatalytic activity of the ZnO/Ag micro/nanospheres

In order to obtain an excellent photocatalyst, the study on the interaction or relationship between photocatalyst and light is essential. So the UV-visible absorption spectrum and photoluminescencee spectra of the ZnO/Ag MNSs were recorded. In Figure 7, the blank test shows that the concentration of MO changes little after irradiation, indicating that the photoinduced self-decomposition can be neglected in comparison with the photocatalysis caused by catalyst particles. Thus, the

UV-light-induced degradation of MO in our work can be evaluated as a real photocatalytic activity of the ZnO/Ag catalyst. When Ag was coupled in ZnO, a remarkable enhancement in photocatalytic activity was observed. A consistent increase in the photocatalytic activity can be noted with the increase in concentration of Ag from 2.5 to 7.5 atom %. However, the photocatalytic activity of the ZnO/Ag decreased as increasing the content of Ag to 10 atom%. The optimal loading of Ag is around 7.5 atom % as the MO is almost completely degraded when irradiated for 30 min. It indicates that an appreciable amount of Ag is necessary to reach the maximum improvement of the photocatalytic activity.

The photodegradation of MO can be considered as a pseudo-first-order reaction[41], and its kinetics can be expressed as:

$$\ln \frac{c_0 - c_t}{c_0} = -kt \quad (1)$$

where C_0 is the initial concentration and C_t is the concentration after the MO degradation for time t. Figure 8 shows the photodegradation curves of MO in the form of $\ln[(c_0 - c_t)/c_0]$ as a function of time and the determined values of the reaction rate constant, k, from linear fitting for different samples. Notably, the ZnO/Ag MNSs exhibit higher photocatalytic activity compared to the pure ZnO. The sample with 7.5 atom % Ag shows the highest catalytic activity with rate constant (k) of 0.1189 min^{-1}, about 6 times more than that of pure ZnO (0.0205min^{-1}), as shown in Figure 8. The improved activity was generally attributed to the efficient charge separation of ZnO/Ag relative to pure ZnO.

To understand the charge transfer mechanism, it is important to note other charge

recombination processes in the materials for which the photoluminescence (PL) spectra of all the samples have been measured and shown in Figure 9. For the pure ZnO, there is a broad strong emission peak in the range 400-600 nm. The emission intensity of ZnO/Ag is suppressed compared with the pure ZnO, duo to Ag deposited on the surface of ZnO microspheres can trap the photogenerated electrons, preventing their recombination with holes. Also it could be seen from the PL spectra that, the emission intensity is decreasing with an increase in concentration of Ag from 2.5 to 7.5 atom %. In addition, the emission intensity increases when the Ag content exceeds 10 atom %. So the optimal Ag content is approximately 7.5 atom %, which is consistent with the above the photodegradation results.

On the basis of the above characterization results, the photocatalytic process of the ZnO/Ag under UV light irradiation can be described as schematically illustrated in Figure 10. As shown in Figure 10(a), when the ZnO/Ag photocatalyst is illuminated, the protruding Ag nanoparticles allow multiple reflections of UV light between the vacant spaces of these Ag nanoparticles, which can make better use of the source light and therefore offer an improved photocatalytic activity[42,43]. As shown in Figure 10(b), in the ZnO/Ag system, when the ZnO absorbs photons of energy greater than or equal to its band gap, electrons jump to the conduction band, creating an equal number of holes in the valence band. Electrons can flow from ZnO to Ag nanoparticles, since the energy level of the conduction band of ZnO is higher than the Fermi level of ZnO-Ag[25-28]. Due to Ag nanoparticles can trap the photogenerated electrons, preventing their recombination with holes. And the deflexed energy band in the space

charge region facilitates the rapid transfer of the as-excited electrons from ZnO to Ag nanoparticles, which increases the lifetime of the photogenerated pairs. Electrons accumulated at Ag particles or the conduction band of ZnO can be transferred to oxygen molecules adsorbed on the surface to form free oxygen radicals, such as $\bullet O^-_2$, $\bullet HO_2$, $\bullet OH$, and so forth, while the photoinduced holes are apt to react with surface-bound H_2O or OH^- to produce the hydroxy lradical species($\bullet OH$), which were extremely strong oxidant for the mineralization of organic chemicals[28-30]. On the other hand, Ag deposited on the surface of ZnO microsphere can absorb UV light, and then emit shorter wavelength light as a result of up-conversion, which in turn further excites ZnO to form electron/hole (e^-/h^+) pairs. The electron/hole pairs then react with the adsorbed oxidants/reducers (usually O_2/OH^-) to produce active oxygen radicals (e.g. $\bullet O_2$, $\bullet OH$), which subsequently cause the degradation of MO[44-46]. The whole process can be expressed as follows[42]:

$$Ag \rightarrow Ag^+ + e^- \quad (2)$$

$$ZnO + hv \rightarrow ZnO + h^+ + e^- \quad (3)$$

$$h^+ + OH^- \rightarrow \bullet OH \quad (4)$$

$$h^+ + H_2O \rightarrow \bullet OH + H^+ \quad (5)$$

$$e^- + Ag^+ \rightarrow Ag \quad (6)$$

$$e^- + O_2 \rightarrow \bullet O_2^- \quad (7)$$

$$\bullet O_2^- + H^+ \rightarrow \bullet O_2H \quad (8)$$

$$2\bullet O_2H \rightarrow H_2O_2 + O_2 \quad (9)$$

3.3. Antibacterial behaviors of the ZnO/Ag micro/nanospheres

The antimicrobial ability of the ZnO/Ag MNSs was tested by the minimum inhibitory concentration (MIC) method as described in Section 2.5 to observe the survival of Escherichia coli cells. Table 1 shows the antibacterial efficiencies of the ZnO/Ag MNSs prepared with different Ag contents against Escherichia coli. The results showed that the tested materials with different Ag content inhibited the bacteria growth at different efficacy, and the pure ZnO has the highest survivability of bacteria. It is clear that the optimal Ag content is approximately 7.5 atom % and the MIC values of ZnO/Ag is 100 $\mu g \cdot mL^{-1}$. Figure 11 shows the photos of agar plates inoculated with bacteria together with different concentrations of ZnO/Ag(7.5 atom% of Ag), in the range of 0 to 150 $\mu g \cdot mL^{-1}$. We can see that the growth of Escherichia coli were completely inhibited as the concentrations of ZnO/Ag is more than 100 $\mu g \cdot mL^{-1}$. There are several reasons to explain that the composite material has excellent antimicrobial property: (1)The Ag nanoparticles dispersedly deposited on the surface of ZnO microsphere make better display of its innate antibacterial activity: a: release of Ag^{+} ions; b: direct attachment onto cell surfaces and promotion of the changes in the membrane permeability; and c: Ag nanoparticles which helps the transfer of photogenerated charge carriers from ZnO produce more reactive oxygen species(ROS), such as: $\bullet O^{-}_{2}$, $\bullet OH$, H_2O_2, to attack the bacterial cells, resulting in cell damage, apoptosis and even death[44-46]. (2) ZnO is also a well-known antibacterial material which is mainly due to its unique activity of photocatalytic bacterial disruption, and partly due to the dissolution of Zn^{2+} ions[20,43]. The photocatalytic disinfection mechanism of ZnO depends on the photo-generated separation of

electrons and holes under irradiation, which can hence produce ROS[44-47]. In addition, The interfacial interaction between Ag and ZnO promoted the separation of charge carriers and hence induced the obvious increase in reactive oxygen species to attack the bacterial cells[46,48]. Such understanding of antibacterial mechanism would primarily establish ZnO/Ag MNSs as a potent broad-spectrum antibacterial agent for its wide applications in various fields.

4Conclusion

Based on a self-design concentric impinging stream microreactor combined microwave technique, a series of ZnO/Ag MNSs with different Ag contents was successfully synthesized by sample, fast, efficient, safe and green method. This composite has excellent photocatalytic and antibacterial activities based on its crystal structure and mophology which will increase the separation rate of the photoinduced electrons and holes. The optimal Ag content is approximately 7.5 atom % as the MO is almost completely degraded when UV light irradiated for 30 min, and the MIC values of ZnO/Ag is 100 $\mu g \cdot mL^{-1}$ which is more smaller than the commercial material. These results showed that the ZnO/Ag MNSs with excellent photocatalytic and antibacterial activities were synthesized, and this highly efficient and large-scale continuous production method has great potential to be extended to the synthesis of other metal-semiconductor materials.

Acknowledgments

The work reported here was supported by the National Natural Science Foundation of China under Grant No.51272117, 51172115, 50972063, the Natural Science

Foundation of Shandong Province under Grant No. ZR2011EMZ001, ZR2011EMQ011, ZR2013EMQ006, the Research Award Fund for Outstanding Young Scientists of Shandong Province Grant No. BS2013CL040, the Specialized Research Fund for the Doctoral Program of Higher Education of China under Grant No. 20123719110003 and the Tackling Key Program of Science and Technology in Shandong Province under Grant No. 2012GGX10218, the Application Foundation Research Program of Qingdao under Grant No. 13-1-4-117-jch,. We express our grateful thanks to them for their financial support.

References

1. L. K. Jagadamma, M. Abdelsamie, A. E. Labban, E. Aresu, N. Ndjawa and D. H. Anjum. J. Mate. Chem. A, 2014, 2, 13321-13331.

2. M. I. Qadir, S. J. Rana, O. Nur, M. Willander, L.A. Larsson and P.O. Holtz. Ceram. Int., 2014, 40, 2435-2439.

3. A.L. Meng , Y. Y. Qiu, L. N. Zhang, X. Xu and Z. J. Li. Sci. China Chem., 2012, 55, 2128-2133.

4. P. Rai, Y. S. Kim, H. M. Song, M. K. Song and Y. T. Yu. Sensor. Actuat. B: Chem., 2012, 165, 133-142.

5. C. Y. Tsay, K. S. Fan, Y. W. Wang, C. J. Chang, Y. K. Tseng and C. K. Lin. Ceram. Int., 2010, 36, 1791-1795.

6. J. F. Huang, C. K. Xia, L. Y. Cao and X. R. Zeng, Mater. Sci. Eng. B, 2008, 150, 187-197.

7. G. H. Kima, D. L. Kima, B. D. Ahna, S. Y. Leeb and H. J. Kima. Microelectr. J., 2009, 40, 272-275.

8. S. C. Pillai, J. M. Kelly, D. E. Mccormack and R. Ramesh. J. Mate. Chem., 2008, 18, 3926-3932.

9. R., Krishna, R. T. Koodali and A. C. Manna. Langmuir, 2011, 27 , 4020-4028.

10. J. M. Yousef and E. N. Danial. J. Health Sci., 2012 , 2, 38-42.

11. Z. E. Karvani and P. Chehrazi. Afr. J. Microbiol. Res., 2011, 5 , 1368-1373.

12. S. Sarkar and D. Basak. CrystEngComm, 2013, 15, 7606-7614.

13. Q. Zhang, Q.H. Zhang and H. Z. Wang. J. Hazard. Mater., 2013, 254 , 318-324.

14. Z. J. Wu, W. H. and K. K. Cui. J. Hazard. Mater., 2014, 278 , 91-99.

15. C. J. Chang, C. Y. Lin and M. H. Hsu. J. Taiwan Insti. Chem. E., 2014, 45, 1954-1963.

16. H. W. Bai, Z. Y. Liu and D. D. Sun. Phys. Chem. Chem. Phys., 2011, 13, 6205-6210.

17. K. S. Shin, K. H. Lee, H. H. Lee, D. Choi and S. W. K. Shin. J. Phys. Chem. C, 2010, 114, 15782-15785.

18. P. Amornpitoksuk, S. Suwanboon, S. Sangkanu, A. Sukhoom, N. Muensit and J. Baltrusaitis. Pow. Technol. 2012, 219, 158-164.

19. M. Ibănescu (Buşilă), V. Muşata, T. Textorb, V. Badilitad and B. Mahltig. J. Alloy. Comp., 2014, 610, 244-249.

20. M. A. Subhan, M. R. Awal, T. Ahmed and M. Younus. Act. Metall. Sin., 2014, 27, 223-232.

21. K. Thongsuriwong, P. Amornpitoksuk and S. Suwanboon. J. Sol-Gel. Sci. Technol., 2012, 62, 304-312.

22. S. Kuriakose, V. Choudhary and B. Satpati. Phys. Chem. Chem. Phys., 2014, 16, 17560-17568.

23. Y. L. Lai, M. Meng and Y. F. Yu. Appl. Catal. B: Environ., 2010, 100, 491-501.

24. J. Wang , X. M. Fan, K. Tian, Z. W. Zhou, Y. Wang. Appl. Surf. Sci.,2011, 57, 7763-7770.

25. Z. J. Li, S. Y. Sun, X. Xu, B. Zheng and A.L. Meng. Cata. Comm., 2011, 12, 890-894.

26. F. Z. Sun, X. L. Qiao and F. T. Tan. J. Mater. Sci., 2012, 47, 7262-7268.

27. A. L. Meng, X. J. Li, X. L. Wang and Z. J. Li. Ceram. Int., 2014, 40, 9303-9309.

28. W. W. Lu, S. Y. Gao and J. J. Wang. J. Phys. Chem. C, 2008, 112, 16792-16800.

29. Q. Deng , X. W. Duan , D. H. L. Ng, H. B. Tang , Y. Yang , M. G. Kong, Z. K. Wu, W. P. Cai and G. Z. Wang. ACS Appl. Mater. & Inter., 2012, 4, 6030-6037.

30. T. Tan, Y. Li, Y. Liu, B. Wang, X. M. Song, E. Li, H. Wang and H. Yan. Mater. Chem. Phys., 2008, 111, 305-308.

31. Z. G. Jia, K. K. Peng, Y. H. Li and R. S. Zhu. T. Nonferr. Metal. Soc., 2012, 22, 873-878.

32. J. Wagner and J. M. Köhler. Nano lett., 2005, 5, 685-691.

33. C. Eamon and M. G. Organ. J. Amer. Chem. Soc., 2005, 127, 8160-8167.

34. X. Zhang, A. D. Terepk and H. Yang. Nano lett.,2004 ,4, 2227-2232.

35. S. Krishnadasan, J. Tovilla and R. Vilar. J. Mater. Chem., 2004, 14, 2655-2660.

36. D. Shalom, R. C. R. Wootton, R. F. Winkle, B. F. Cottam, R. Vilar, A. J. Demello and C. P. Wilde. Mater. Lett., 2007, 61, 1146-1150.

37. D. D. Lin, H. Wu, R. Zhang and W. Pan. Chem. Mater., 2009, 21, 3479-3484.

38. M. Kunat, S. G. Girol, U. Burghaus and C. Woll. J. Phys. Chem. B, 2003, 107, 14350-14356.

39. C. D. Gu, C. Cheng, H. Y. Huang, T. L. Wong, N.Wang and T. Y. Zhang.Cryst. Grow. Desig., 2009, 9, 3278-3285.

40. Y. H. Zheng, L. R. Zheng, Y. Y. Zhan, X. Y. Lin, Q. Zheng and K. M. Wei. Inorg. Chem., 2007, 46, 6980–6986.

41.C. L. Ren, B. F. Yang, M. Wu and J. Xu. J. Hazard. Mater., 2010, 182, 123-129.

42. S. N. Baker and G. A. Baker. Angew. Chem. Int. Edit., 2010, 49, 6726-6744.

43. H. T. Li, R. H. Liu and Y. Liu. J. Mater. Chem., 2012, 22,17470-17475.

44. Y. Zhang, X. J. Gao and L. Zhi. J. Inorg. Biochem., 2014, 130, 74-83.

45. H. R. Panta, D. R. Pandeyac and K. T. Namd. J. Hazard. Mater., 2011, 189, 465-471.

46. C. Karunakaran, V. Rajeswari and P. Gomathisankar. J. Alloy. Comp., 2010, 508, 587-591.

47. A. Kumar, P. K. Vemula, P. M. Ajayan and J. George. Nature mater., 2008, 7, 236-241.

48. S. C. Motshekgaa, S. S. Raya and M. S. Onyango, J. Hazard. Mater., 2013, 262, 439-446.

Figure Captions

Figure 1. Schematic diagram of the experimental set-up: A, B. reaction solutions, C. concentric impinging streams microreactor , D. the precursor solution ,1 , 2 inlets.

Figure 2. Flowchart schematic for synthesis of the ZnO/Ag micro/nanospheres

Figure3. XRD patterns of the ZnO/Ag micro/nanospheres recorded at different Ag contents. Peaks marked by (asterisk) are indexed to the fcc Ag

Figure 4. The SEM, TEM and HRTEM images of ZnO/Ag micro/nanospheres with Ag-7.5 atom % (a) low-magnified SEM image (the inset shows the EDS spectrum of ZnO/Ag), (b) low-magnified TEM image, (c) HRTEM image, (d) HRTEM image from the squared region (C) of part c and the two insets are the selected area electron diffraction (SAED) patterns corresponding to Ag and ZnO, respectively.

Figure 5. Growth mechanism of Ag nanoparticle decorated ZnO microspheres

Figure 6. XPS spectra of the ZnO/Ag MNSs obtained in the presence of 7.5 atom % Ag: (a) XPS

full spectrum of the sample, (b) Zn $2p_{3/2}$ spectrum, (c) O 1s spectrum, and (d) Ag 3d spectrum.

Figure 7. The photodegradation of MO by the ZnO/Ag micro/nanospheres with different Ag contents under ultraviolet irradiation

Figure 8. Kinetic curves for the photodegradation of MO by the ZnO/Ag micro/nanospheres with different Ag contents under UV light irradiation

Figure 9. PL spectra of ZnO/Ag micro/nanospheres prepared with various Ag contents

Figure 10. The Proposed photocatalytic mechanism of the ZnO/Ag micro/nanospheres

Figure 11. Photos of agar plates inoculated with bacteria together with ZnO/Ag micro/nanospheres(a: 0 $\mu g \cdot mL^{-1}$,b: 25 $\mu g \cdot mL^{-1}$,c:50 $\mu g \cdot mL^{-1}$,d:100 $\mu g \cdot mL^{-1}$, e:150 $\mu g \cdot mL^{-1}$).

Figure

Figure 1

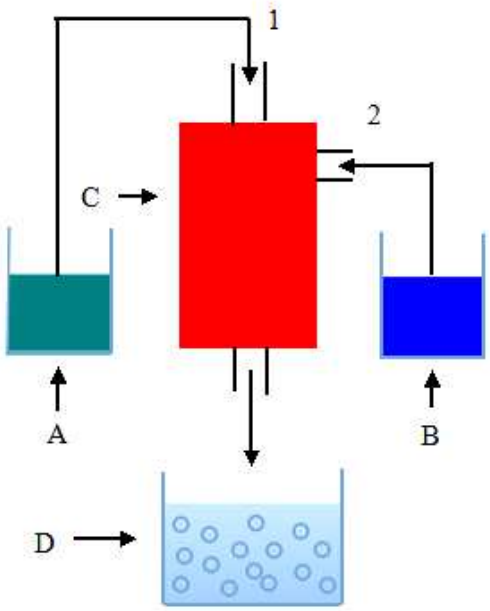

Figure 2

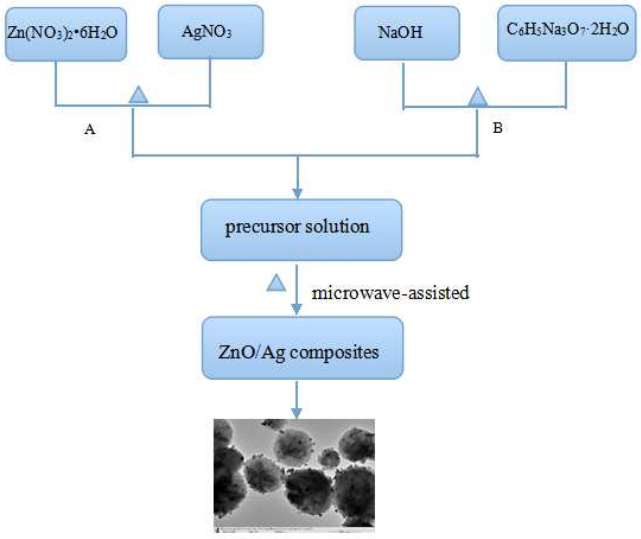

Figure 3

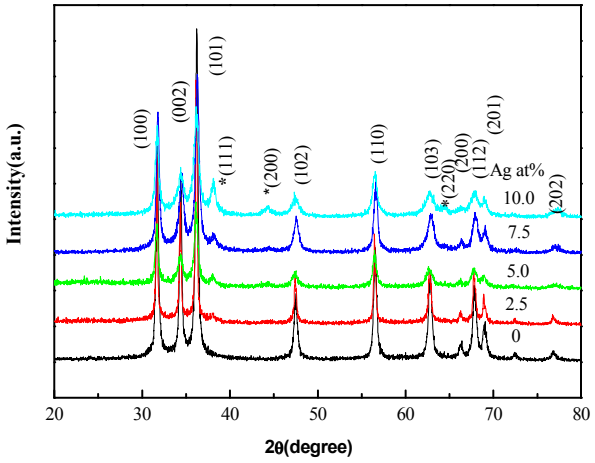

Figure 4

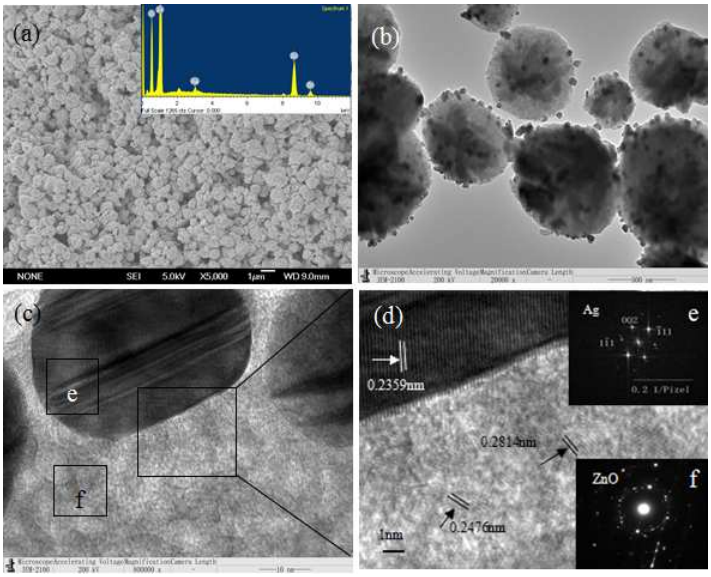

Figure 5

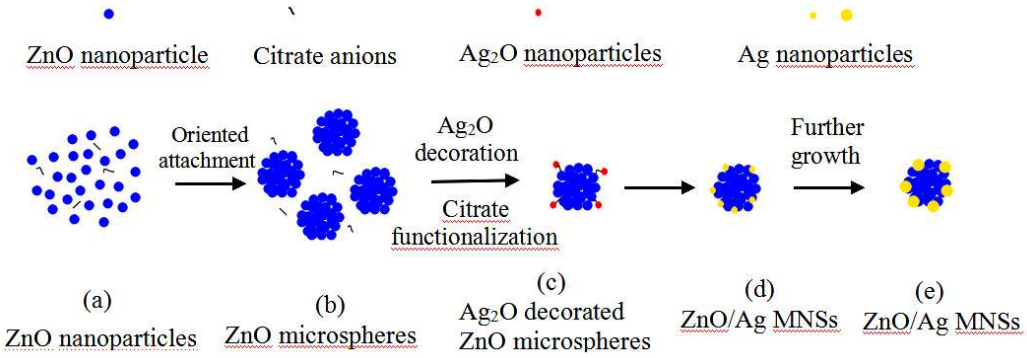

Figure 6

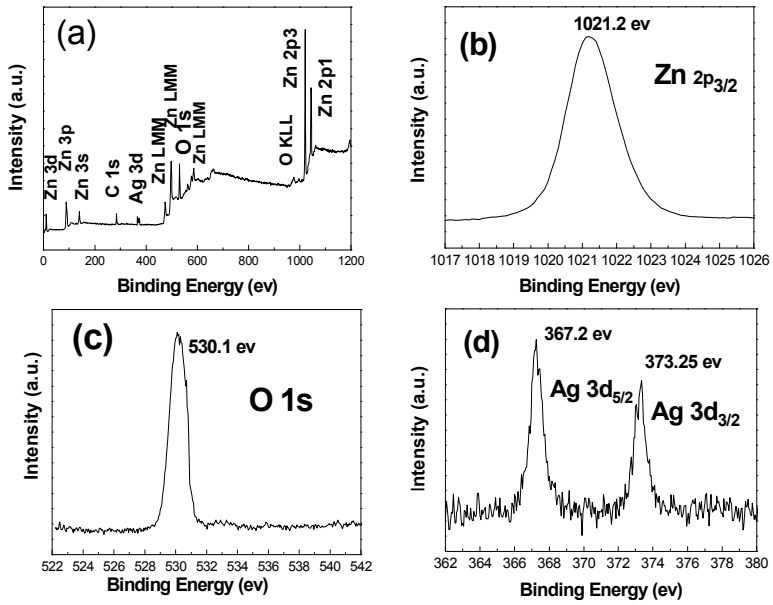

Figure 7

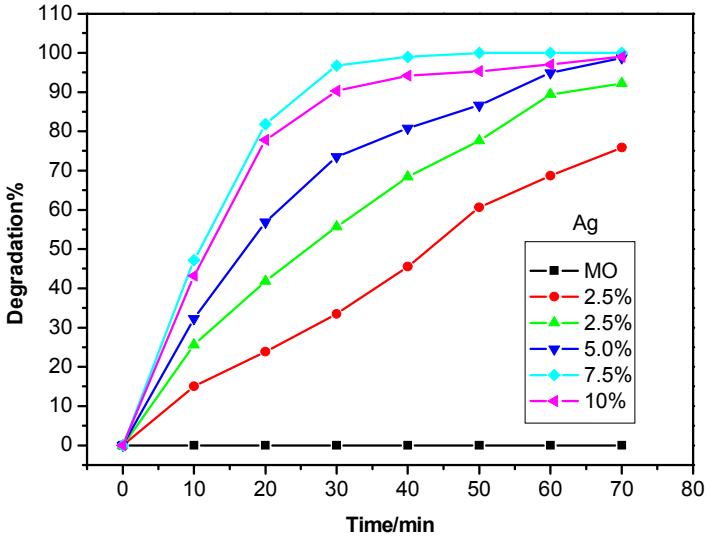

Figure 8

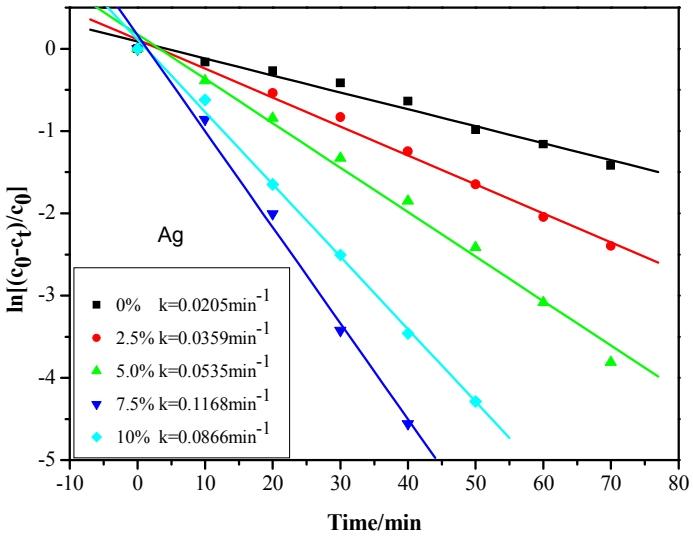

Figure 9

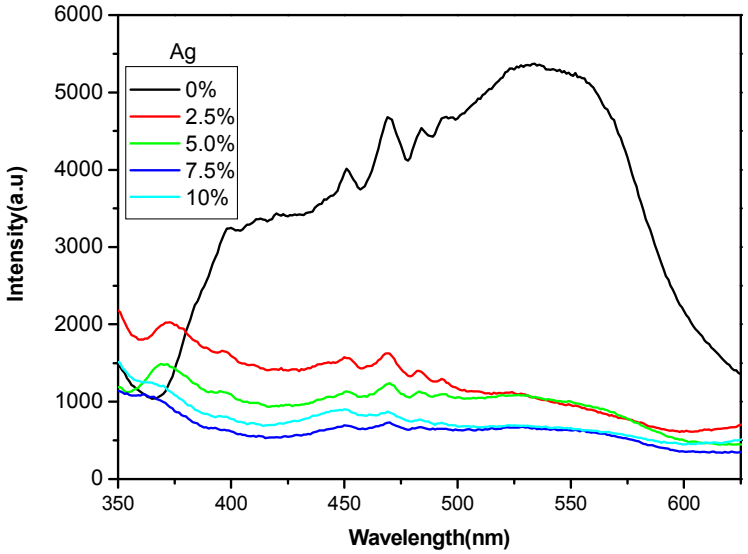

Figure 10

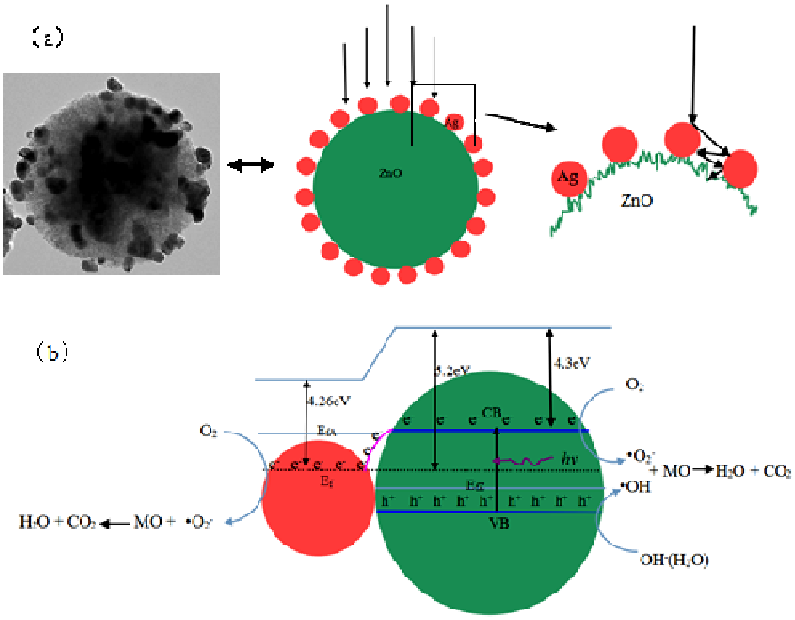

Figure 11

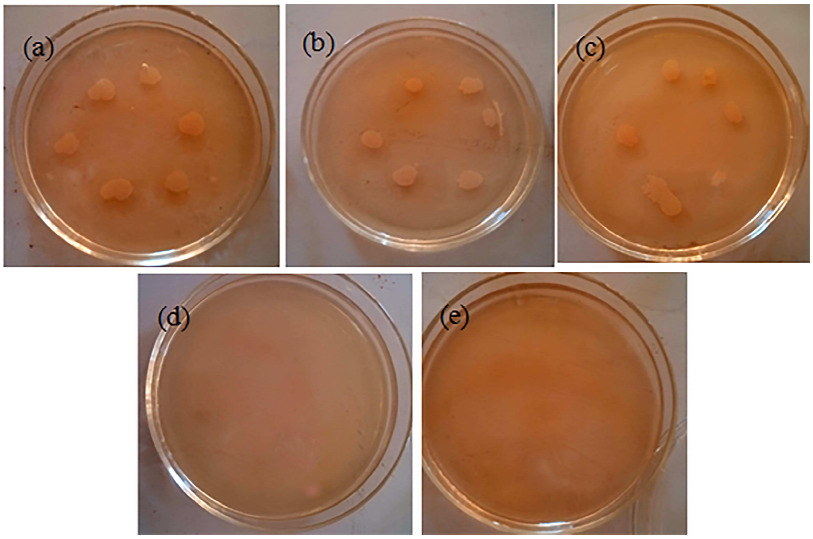

Table

Table 1

Concentration of ZnO/Ag ($\mu g \cdot mL^{-1}$)	different Ag contents				
	0	**2.5%**	**5%**	**7.5%**	**10%**
50	+	+	+	+	+
100	+	+	+	_	+
150	+	+	+	_	_
200	+	+	_	_	_
300	+	+	_	_	_
400	+	_	_	_	_
500	_	_	_	_	_

Table 1. Measures of bacterial inhibition of Escherichia coli with different Ag contents:

+ : with Escherichia coli growth , - : without Escherichia coli growth.